Supplementary materials

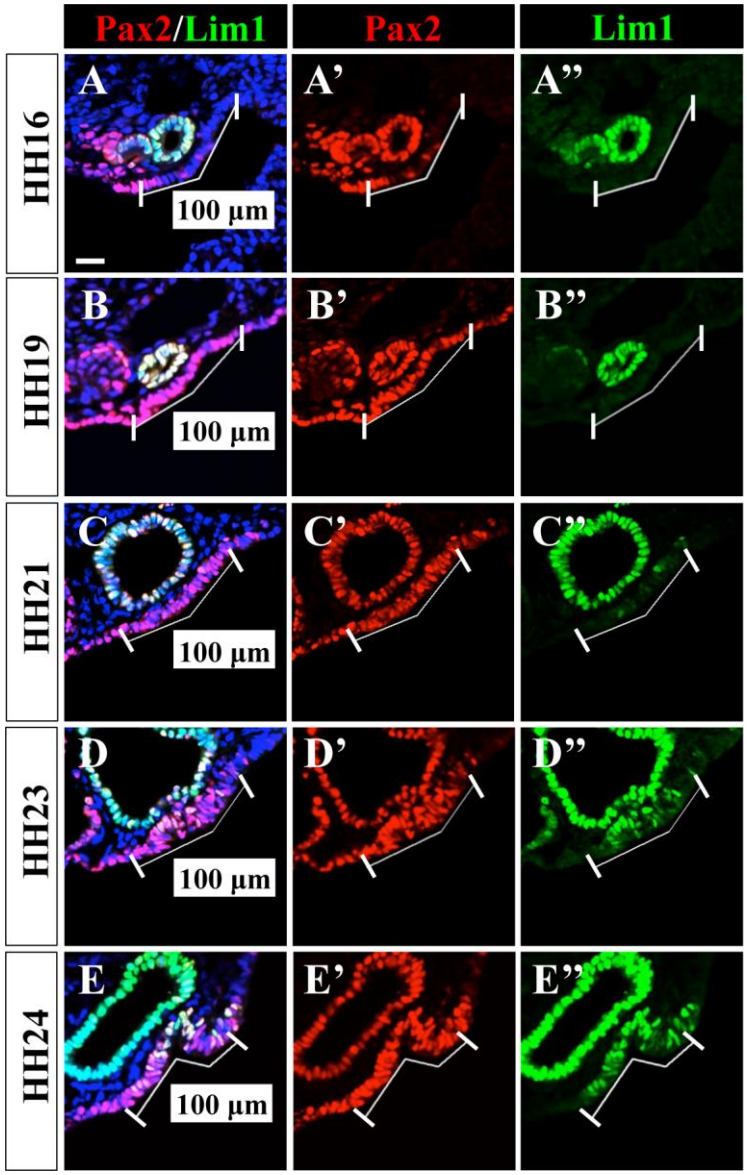

Figure S1

Definition of the Müllerian duct forming region (MFR). (A-E) The range measuring 100 µm laterally from medial edge of WD in coelomic epithelium was defined as MFR at each stage. Scale bar: 20 µm in A.

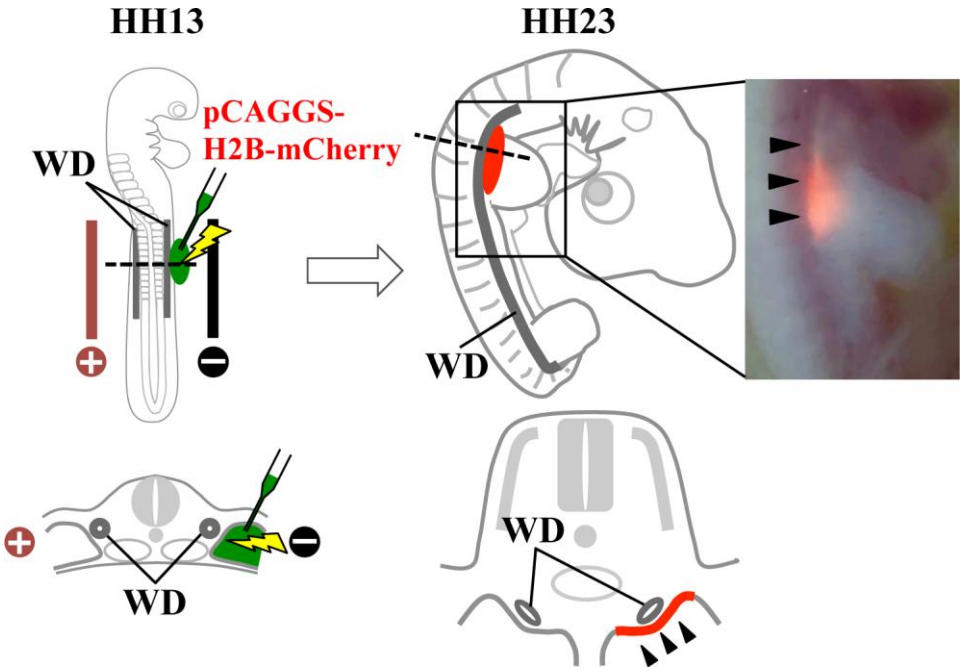

Figure S2

Diagrams illustrating procedures of in ovo electroporation into MFR. A DNA solution (pCAGGS-H2B-mCherry) shown in green was injected into the coelomic cavity of HH13 embryos. Horizontally positioned electrodes are indicated as + (anode, red) and – (cathode, black). The photo shows mCherry signals seen in presumptive MD of an HH23 embryo (arrowheads).

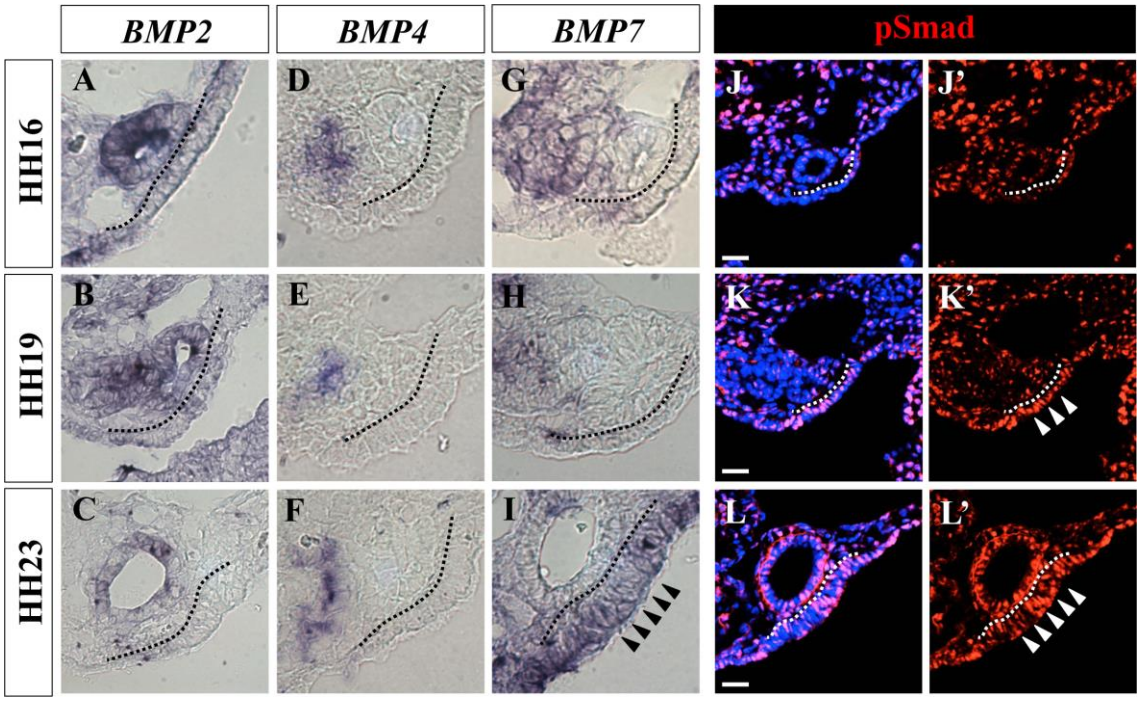

Figure S3

Expression patterns of BMP2/4/7 in the mesonephric region, and activation of Smad1/5/8 in MFR. (A-I) *In situ* hybridization to show expression of *BMP2* (A-C), *BMP4* (D-F) and *BMP7* (G-I) in HH16, HH19 and HH23 embryos. Arrowheads in I indicate *BMP7* expression in MFR. (J-L) Immunostaining for phosphorylated Smad1/5/8 (pSmad). Signals for pSmad were detected at HH19 and HH23 (white arrowheads in K', L'). Scale bars: 20 μm in J, K, L.

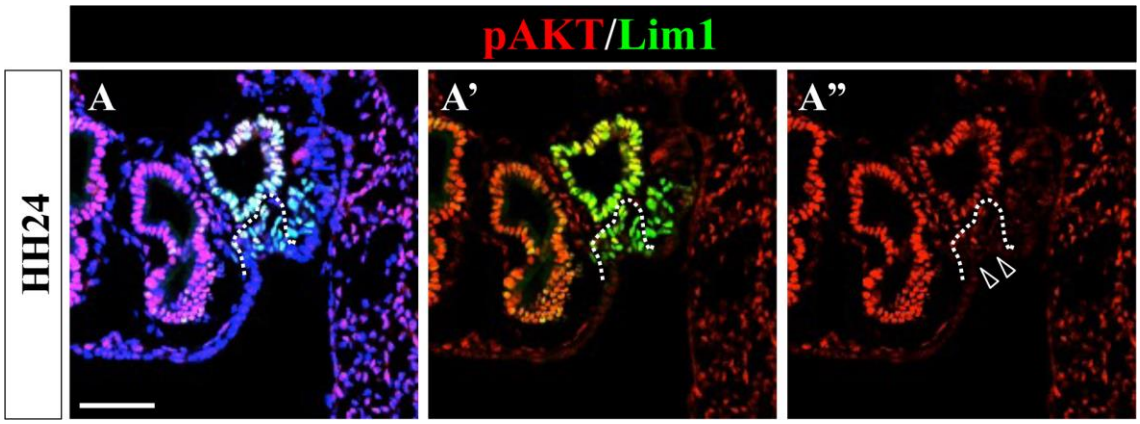

Figure S4

Immunostaining against phosphorylated AKT (pAKT). (A) Open arrowheads in A" show no signal of pAKT in MD precursors at HH24. Scale bar: 100 μm.

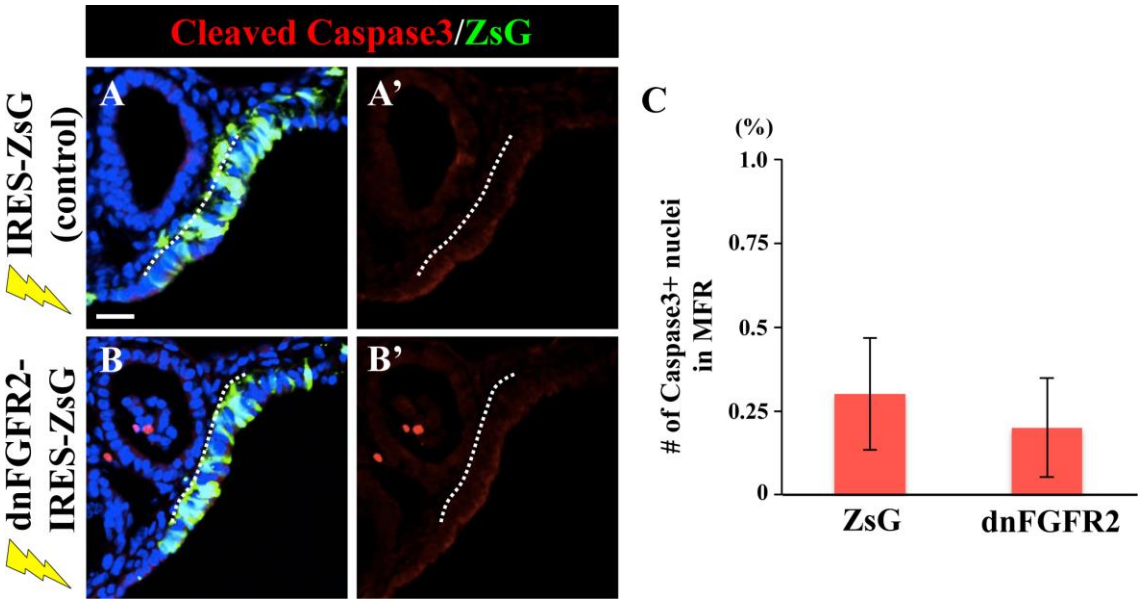

Figure S5

Inhibition of FGF signaling did not affect cell survival. (A, B) Transverse sections of ZsG- (control; A) or dnFGFR2-electroporated HH23 embryos (B) were stained with antibodies for cleaved Caspase3 (red) to visualize apoptotic cells. (C) Quantification of apoptotic cells within ZsG- or dnFGFR2-electroporated MFRs (n = 10 each). Inhibition of FGF signaling by dnFGFR2 did not excessively induce cell deaths. Error bars represent SEM. Scale bar: 20 μm in A.

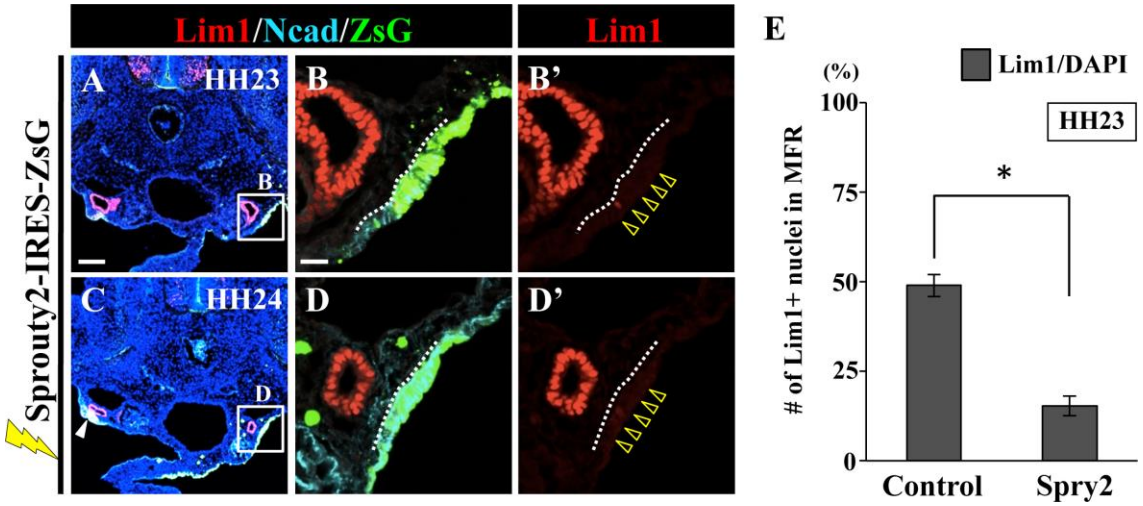

Figure S6

Misexpression of Sprouty abrogated the specification and invagination of MD precursors. (A-D) Sections of HH23 and HH24 embryos electroporated with *Sprouty2* cDNA (n = 12 for each stage). Signals for Lim1 (red) were not detected in the electroporated MFRs as indicated by yellow open arrowheads. (E) Quantitative representation of the number of Lim1-positive cells in ZsG-electroporated- and Sprouty2-electroporated MFR in HH23 embryos. Error bars represent SEM. *$p < 0.01$. Scale bars: 100 μm in A; 20 μm in B.

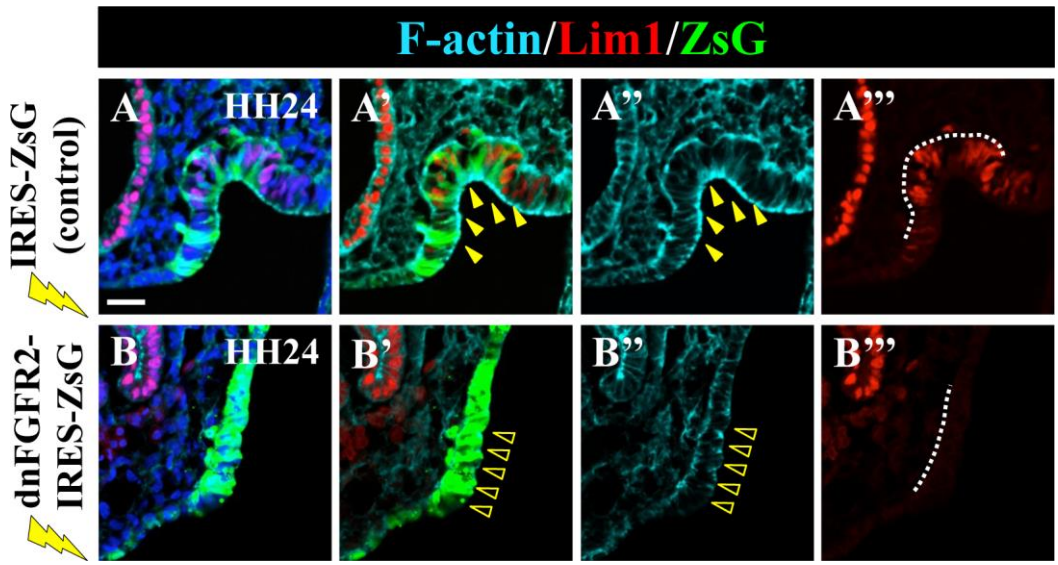

Figure S7

F-actin organization of MFR was controlled by FGF signaling. (A-B) F-actin (cyan) was depleted in dnFGFR2-electroporated MFR of HH24 embryo (open arrowheads in B; n = 8). Scale bar: 20 μm in A.

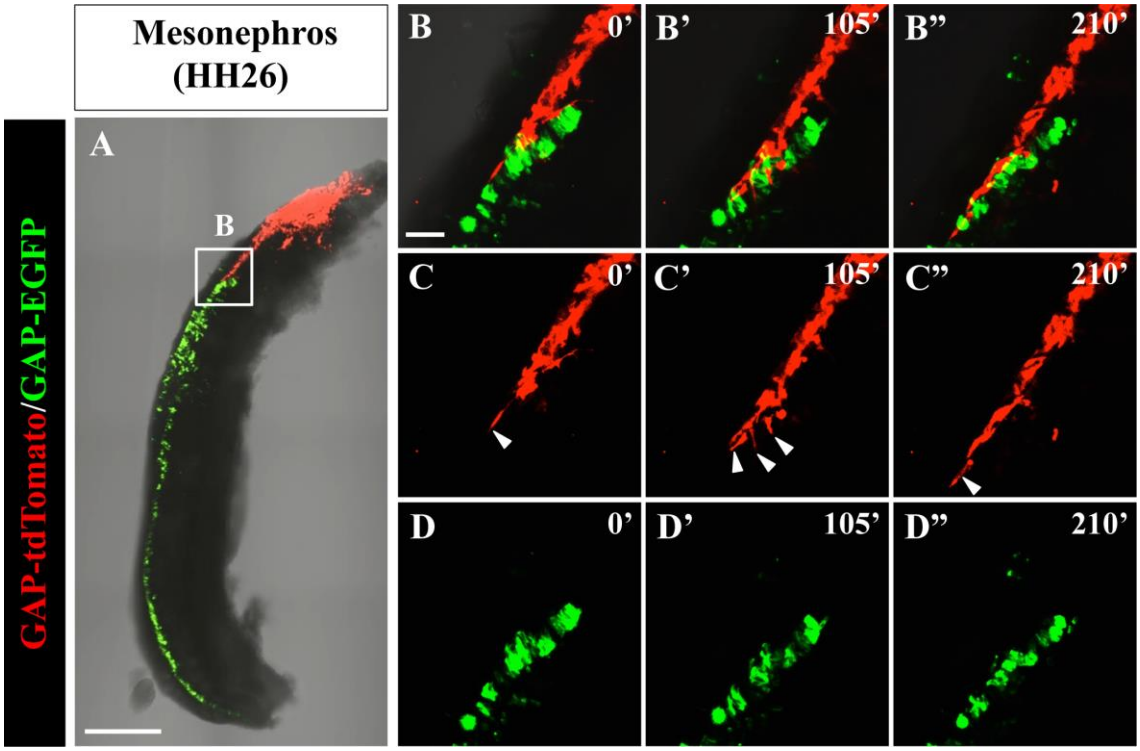

Figure S8

Time-lapse images of elongating MD. (A) A mesonephros explant from HH26 embryo was cultured *in vitro*, and imaged for 210 min. (B-D) Selected frames from the time-lapse movie (Movie S1) showing that GAP43-tdTomato-electroporated MD cells (red) migrated along GAP43-EGFP-electroporated WD (green). Pseudopodia were observed on leader cells of MD as indicated by white arrowheads in (C). Scale bars: 500 μm in A; 50μm in B.

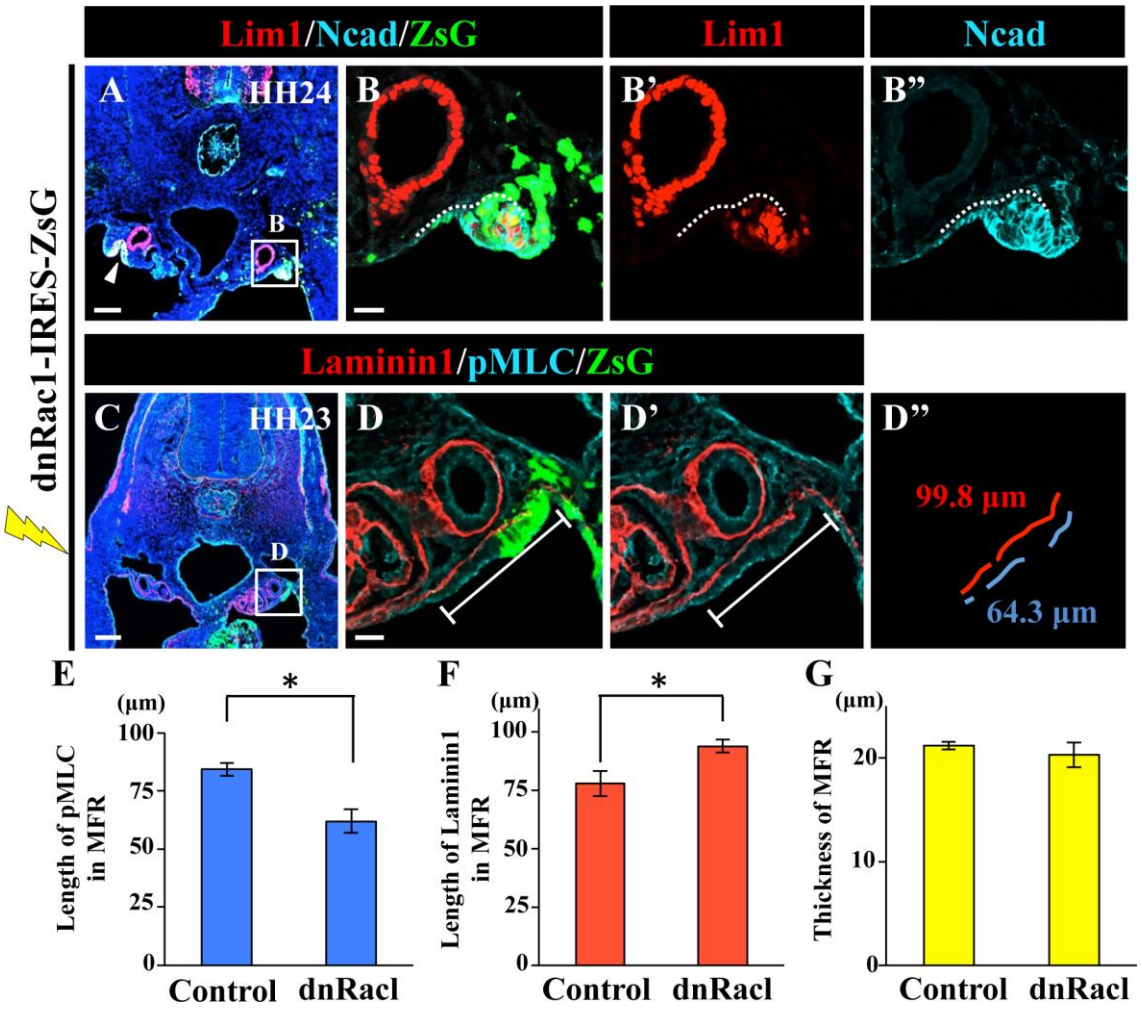

Figure S9

Implication of Rac1 in MD invagination. (A, B) A dominant negative form of Rac1 (dnRac1) electroporation caused a failure of MD invagination (n = 15). Note that misexpression of dnRac1 did not significantly affect Lim1 expression in MD precursors. (E-G) Graphs showing pMLC-length (E), Lamin1-length (F) and thickness (G) of IRES-ZsG- and dnRac1-IRES-ZsG electroporated MFRs (n = 10 each). Error bars represent SEM. *$p < 0.05$. Scale bars: 100 µm in A, C; 20 µm in B, D.

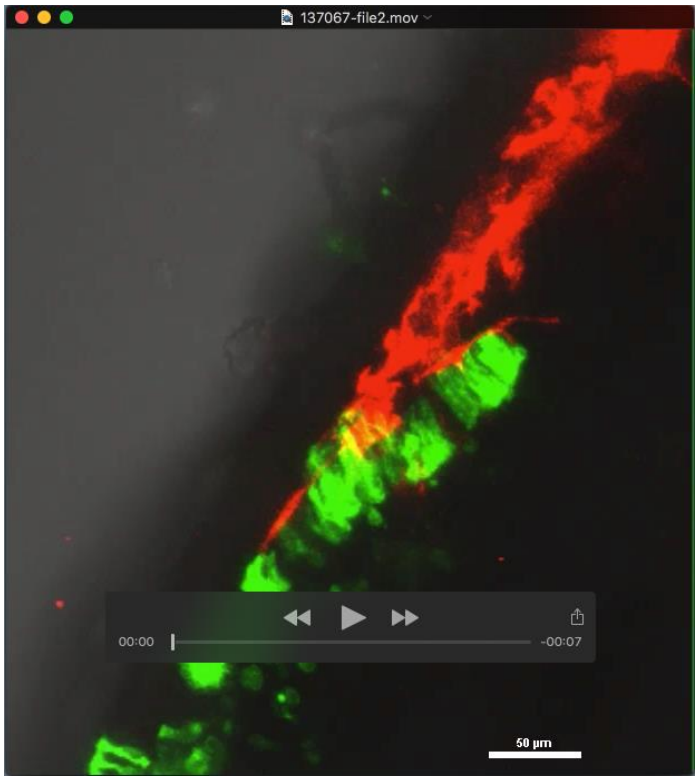

Movie S1

Time-lapse analyses using a cultured mesonephros where GAP-tdTomato (red) and GAP-EGFP (green) were electroporated into MD and WD, respectively. This movie corresponds to Fig. S8. Frames were taken every 3 min with a 20 x Plan-Apochromat objective lens. Total movie length: 210 min.